A semi-flexible tetrahydrazone macrocycle for binding of pyrophosphate and smaller anions

Lau Halgreen,[a] Aaron Torres-Huerta,[a] Karolis Norvaisa,[a] Gaël De Leener,[b] Nikolay Tumanov,[c] Johan Wouters,[c] Kristin Bartik,[a] Hennie Valkenier[a]

a. Université libre de Bruxelles (ULB), Engineering of Molecular NanoSystems, Ecole polytechnique de Bruxelles, Avenue F.D. Roosevelt 50, CP165/64, B-1050 Brussels, Belgium.
b. Centre d'Instrumentation en REsonance Magnétique (CIREM), Université libre de Bruxelles (ULB), Avenue F. D. Roosevelt 50, CP 160/08, B-1050 Brussels, Belgium.
c. Namur Institute of Structured Matter and Namur Research Institute for Life Sciences, Department of Chemistry, University of Namur, 61 rue de Bruxelles, B-5000 Namur, Belgium

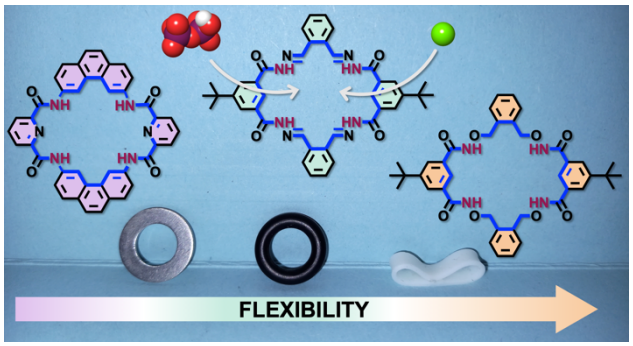

Abstract:

Macrocyclization has proven to be a useful design strategy in the development of efficient anion receptors. In addition to ring size, the overall preorganization by structural rigidity is of key importance. To explore this in the context of developing an efficient pyrophosphate receptor, three macrocycles featuring a 26-membered interior ring size and similar H-bonding motifs have been synthesized and their anion binding ability investigated. Computational studies and NMR data showed different degrees of preorganization as a result of differences in flexibility. The interaction of the three macrocycles with chloride, dihydrogenphosphate, and dihydrogen pyrophosphate was investigated in solution by NMR and UV-Vis spectroscopy, and in the solid state by X-ray crystallography. The tetrahydrazone based macrocycle featuring intermediate flexibility exhibited the best affinity for all three anions investigated. Our results suggest that in addition to the proper preorganization of binding groups in a macrocycle a certain degree of flexibility is also required for an optimal affinity with the target guest.

Introduction

Anion recognition is at the basis of processes such as sensing or transmembrane transport. [1–4] The recognition of phosphate species is of particular interest in the biological field. Various phosphate species play important roles in a wide range of biological processes, including encoding of genes, energy storage, and as a crucial building block for bones and teeth.[5] Furthermore, phosphate species can also be linked to diseases such as hyperphosphatemia, characterized by increased levels of phosphate in the blood,[6] or pseudogout, a form of arthritis caused by calcium pyrophosphate dihydrate (CPPD) deposits.[7,8] Pyrophosphate in serum is formed primarily by the hydrolysis of ATP, while it is in turn hydrolysed to inorganic phosphate. Pyrophosphate is essential to control mineralisation, avoiding undesired calcium phosphate (hydroxyapatite) formation, while growing CPPD crystals at elevated pyrophosphate levels.[7–9] As a result of the importance of phosphate species, receptors capable of effectively binding, sensing, or transporting these species are of great interest. [10–14]

One of the most common approaches for the development of phosphate and pyrophosphate receptors has been the use of NH- or OH-based H-bond donors, mimicking the way that natural receptors achieve phosphate recognition.[15–17] It is well established that the proper preorganization of the molecular structure contributes to the affinity.[18–20] A macrocyclic approach is therefore often used. Size complementarity between receptor and substrate was shown early on by Dietrich *et al*. to have a significant effect on the stability of cryptand anion complexes,[21] and numerous other contributions have ensued this seminal work. Focussing on neutral tetralactam-based macrocycles as anion receptors, Chmielewski and Jurczak have shown that the size of macrocyclic receptors plays an essential role in both the selectivity and strength of receptor-anion interactions.[22,23] Their work also showed that pyridyl N-atoms in dipicolinic bisamides contribute to the preorganization of the amides for anion binding, resulting in significant increases in binding affinities compared to isophthalamides.[22] The comparison of the 18-membered tetralactam receptor with ethylene spacers of Szumna and Jurczak [24] with its aromatic and rigid counterpart prepared by Smith and co-workers[25] seems to support the notion that more rigid macrocycles lead to higher anion affinities. Similarly, Flood and co-workers obtained higher binding affinities with more rigid triazole based anion receptors compared to their more flexible counterparts.[26] On the other hand, some examples can also be found where an increase in flexibility within a macrocyclic structure can be beneficial for binding, such as the work carried out by Glas *et al.* in which they investigated the effect of conformational flexibility of two similar peptide based macrocyclic receptor on the stability of the corresponding macrocycle-ligand complexes. The most flexible of the two showed the highest affinity.[27]

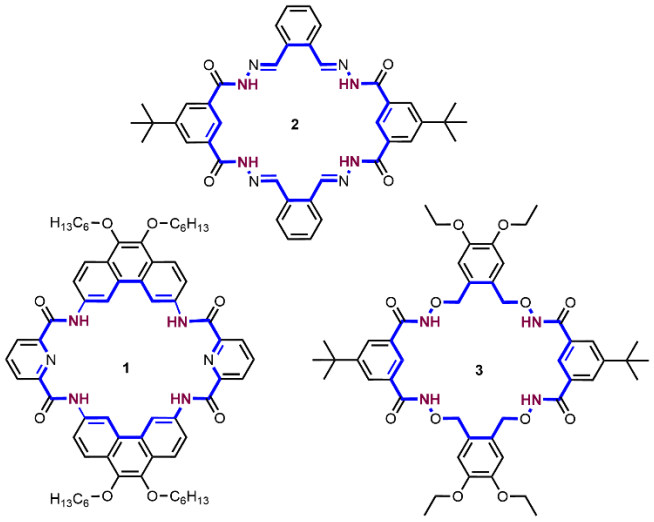

Figure 1. The three macrocycles synthesized and investigated in this work, all with an interior macrocycle size of 26 atoms (blue) and four NH groups as H-bond donors (dark red).

With this notion of the importance of size, flexibility, and preorganization in mind, we set out to develop a series of macrocyclic receptors for dihydrogen pyrophosphate ($H_2P_2O_7^{2-}$), exhibiting identical macrocyclic ring sizes and possessing in all cases four NH-based hydrogen bond donors. Here, we describe the design, synthesis, and

characterization of macrocycles **1**, **2**, and **3** (Figure 1) and their ability to bind $H_2P_2O_7^{2-}$, as well as the smaller anions $H_2PO_4^-$ and Cl^- in solution and in the solid state.

Results and discussion

Macrocycle design and molecular modelling

Previously reported neutral macrocyclic receptors for $H_2P_2O_7^{2-}$ have utilized 24- and 32-membered molecular scaffolds to achieve anion binding.[28,29] With the help of computational studies we found that 26-membered macrocycles would allow the design of D_{2h} symmetric structures with binding cavities showing good size complementarity for $H_2P_2O_7^{2-}$.

Three different macrocycles with an increasing degree of flexibility, but all with 26 atoms in the macrocyclic ring were designed as anion receptors to find the optimal compromise between preorganization and flexibility (Figure 1). Macrocycle **1** was designed to be the most rigid of the three. It employs dipicolinic bisamides, which are known to prefer a *syn-syn* configuration due to interactions of the amide NH and the lone pair on the pyridyl N,[22,23,30,31] as well as phenanthrene spacers to give rigidity and the desired appropriate macrocyclic ring size. This in turn was envisaged to result in preorganization of the amides to accommodate $H_2P_2O_7^{2-}$ in the binding cavity. Macrocycle **2** was designed to be more flexible, replacing the dipicolinic bisamide motif with isophthalic acylhydrazones. This could potentially also lead to interactions from the CH proton of the isophthalic subunit between the two acylhydrazones, which has been reported to be able to participate in anion binding.[25,32,33] Macrocycle **3**, employing bis-N-(benzyloxy)isophthalamides, was designed to be the most flexible. The *n*-hexyl and ethyl ether groups of **1** and **3** respectively, as well as *tert*-butyl groups of **2** and **3** are present to enhance the solubility of the macrocycles in organic solvents as required for anion binding studies.

Macrocycles **1**-**3** have four NH H-bond donating groups at the same positions in the macrocycles. However the groups of these three macrocycles vary from acylhydrazones to (N-alkoxy)amides, which could potentially lead to differences in binding between the three macrocycles. To try and gauge the influence of these H-bond donors on anion affinity, both literature data[34,35] on anion binding of these functional groups as well as their estimated pK_a were considered (see SI for details). It appears that the available anion binding data as well as the pK_a values of the moieties in question are not too different and thus not likely to be the main source of observed differences

Computational studies using a semi-empirical PM7 approach in MOPAC were carried out for each of the three receptors without guest, with $H_2P_2O_7^{2-}$, and with the much smaller Cl^- anion to gain insights in the differences in the conformation of the receptors. In the absence of any guest (Figure 2a-c), macrocycle **1** adopts a preferred conformation with all the NHs pointing into the cavity, suggesting a good preorganization for $H_2P_2O_7^{2-}$ binding. Macrocycle **2** adopts a preferred conformation with two of the NH groups pointing into and the other two pointing out the cavity. Macrocycle **3** exhibits intramolecular H-bonding, with two of the NH protons interacting with carbonyl groups pointing towards the interior of the cavity and the other two NH protons pointing outwards.

In the presence of $H_2P_2O_7^{2-}$, all three macrocycles were able to adopt conformations in which all four H-bond donors are interacting with the guest (Figure 2d-f), however with different NH to O bond lengths: the NH to O distances fall within the range of 1.47-1.80 Å with averages of 1.64 Å and 1.70 Å for macrocycles **2** and **3** respectively, whereas the average H-bond length of macrocycle **1** is 1.88 Å. Macrocycles **2** and **3** can furthermore adapt their conformation to have all four NH groups interacting with a smaller Cl^- anion (Figure 2h and 2i, NH to Cl distances of 2.19-2.35 Å), while the more rigid macrocycle **1** is unable to utilize all four NH groups to interact with the Cl^- anion, which is thus located at one of the two dipicolinic bisamide sites (Figure 2g, NH to Cl distances of 1.99 and 2.03 Å).

These computational studies confirm that macrocyle **1** is most preorganized for $H_2P_2O_7^{2-}$ binding, with all NH groups pointing into the cavity. However, its rigidity hinders it from forming four H-bonds to the small Cl^- anion. Macrocycle **2** is less preorganized than **1**, with only two NH groups pointing into the cavity in its lowest energy conformer, but it can adapt its conformation to bind $H_2P_2O_7^{2-}$ or Cl^- with all NH groups. Macrocycle **3** is least

preorganized for anion binding with intramolecular H-bonds closing the cavity in absence of a guest, but it has a good adaptability to anionic guests of different sizes. Note that only NH protons are shown in Figure 2 but that CH protons pointing into the cavity could also contribute to anion binding.

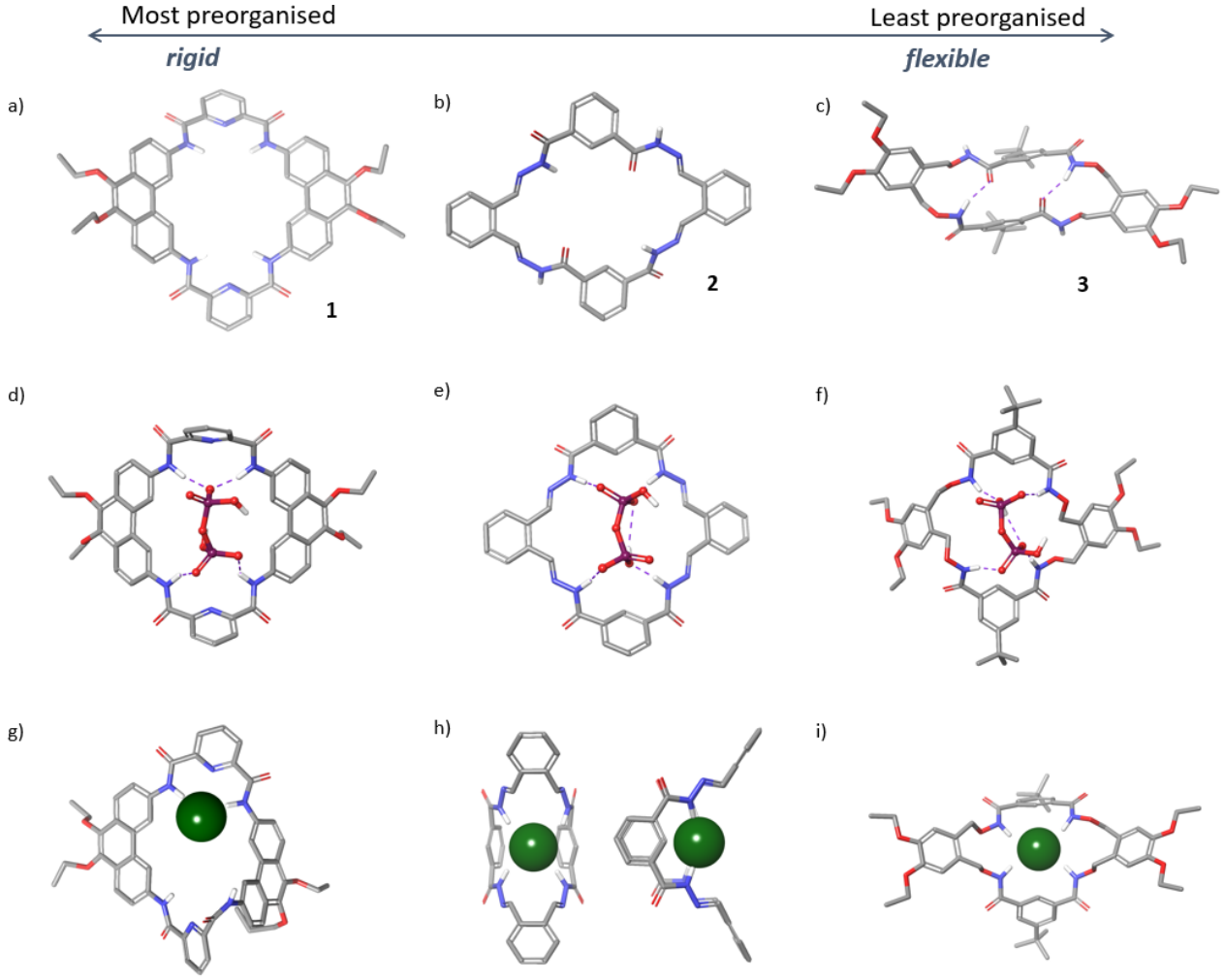

Figure 2. Molecular models (PM7 optimized geometries, vacuum) of lowest energy conformations of macrocycles **1**-**3** without anions (a-c), with $H_2P_2O_7^{2-}$ (d-f) and Cl^- (g-i).

Synthesis

Macrocycle **1** was synthesized by the condensation of diacylchloride **8**[36] with 3,6-diamino-9,10-dihexoxyphenanthrene **7** (Scheme 1). Diamino-phenanthrenes with this substitution pattern have not been reported to date but could be useful building blocks in organic synthesis for various applications. While 3,6-diamino-9,10-dihexoxyphenanthrene **7** could not be obtained in pure form as the free base due to its propensity to decompose, a synthesis route to obtain the HCl salt of **7** in three steps from commercially available 3,6-dibromophenanthrene-9,10-dione **4** was developed. This route starts by reductive etherification of **4** to get 3,6-dibromo-9,10-dihexoxyphenanthrene **5**,[37] followed by a Buchwald-Hartwig cross coupling with benzophenone imine **6** and subsequent acid hydrolysis of the formed bisimine. The reaction between the HCl salt of phenanthrenediamine **7**·2(HCl) and diacylchloride **8** in the presence of DIPEA as base affords the desired macrocycle in around 10% yield. However, addition of 45 equivalents of tetrabutylammonium chloride (TBACl) improved the yield significantly and facilitated purification by column chromatography due to the better solubility of **1** in the presence of TBACl. Additional optimization steps such as slow addition of reagents and performing the reaction in the dark and under an argon atmosphere to try and prevent decomposition of the free base of **7**·2(HCl) ultimately improved the yield to 27%.

Scheme 1. Synthetic scheme for the synthesis of macrocycle **1**.

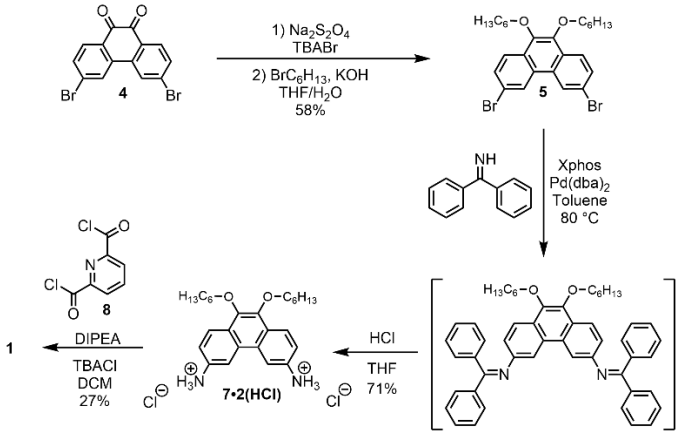

Macrocycle **2** was synthesized by the condensation of bishydrazide **10**[38] with phthalaldehyde **11** in the presence of $TBAH_2PO_4$ in 57% yield (Scheme 2). The $H_2PO_4^-$ template proved to be essential since, when absent, the macrocycle was obtained as a mixture with larger macrocycles and oligomers which could not be separated, whereas the presence of $TBAH_2PO_4$ caused the desired macrocycle to selectively precipitate from solution.

Scheme 2. Synthetic scheme for the synthesis of macrocycle **2**.

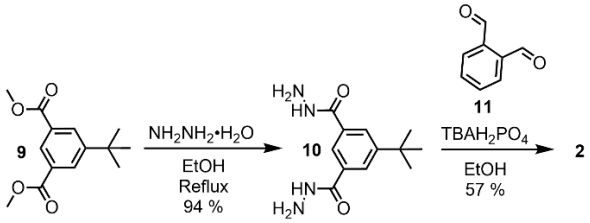

Finally, macrocycle **3** was synthesized in a similar manner as macrocycle **1** by condensation of *bis*-*O*-hydroxylamine **16** with diacylchloride **17**[39] (Scheme 3). The bis-*O*-hydroxylamine was obtained in three steps by bromomethylation of 1,2-diethoxybezene **12**, followed by nucleophilic substitution by N-hydroxyphthalimide **14**[40] on **13**[41] and subsequent hydrazinolysis. Notably, for this macrocyclization, the rate of addition had little effect on the yield of the reaction, and increasing the equivalents of TBACl beyond 10 only had a negligible effect on the yield. Moreover, the addition of other templates such as $TBAH_2PO_4$ or $TBA_2H_2P_2O_7$ gave lower yields compared to the 55% yield obtained with TBACl.

Scheme 3. Synthetic scheme for the synthesis of macrocycle 3.

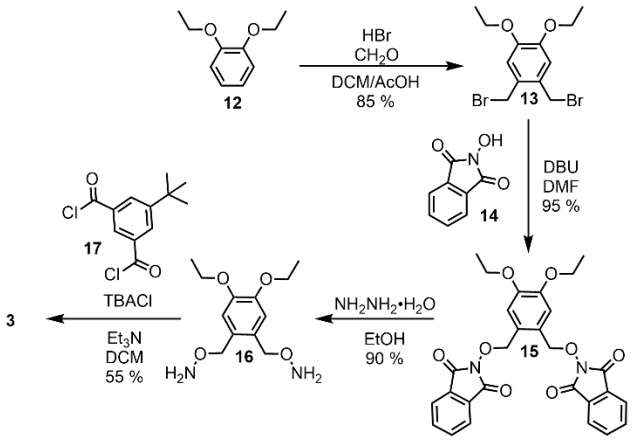

Attempts were made at condensing diaminophenanthrene **7** with diacylchloride **17** or glutaryl chloride, at condensing phthalaldehyde **11** with bisacylhydrazines derived from dipicolinic acid or glutaric acid, and at condensing *bis*-O-hydroxylamine **16** with diacyl chloride **8**, but the desired macrocycles were either not observed or the purification was unfeasible.

NOE studies

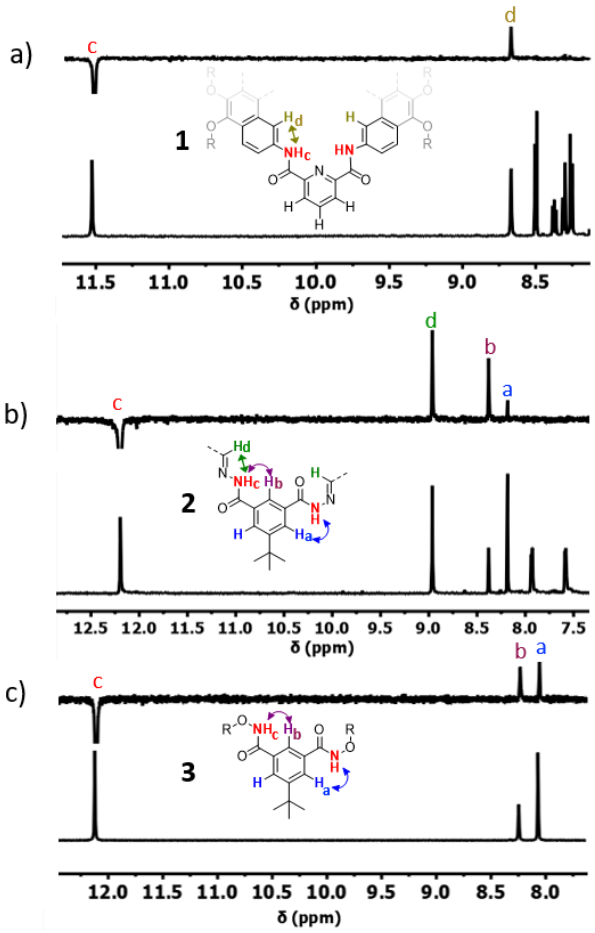

Figure 3. 1D-ROESY (top) and ^{1}H-NMR spectrum (bottom) of a) macrocycle **1** (600 MHz, DMSO-d_6 + 0.5% H_2O, 1D-ROESY mixing time = 200 ms) with interaction observed between proton H_c and H_d; b) macrocycle **2** (600 MHz, DMSO-d_6 + 0.5% H_2O, 1D-ROESY mixing time = 200 ms) with interactions observed between proton H_c and H_d, H_b, and H_a; c) macrocycle **3** (400 MHz, DMSO-d_6 + 0.5% H_2O, 1D-ROESY mixing time = 250 ms) with interactions observed between proton H_c and H_b and H_a.

Upon obtaining the three macrocycles, their difference in preorganization and conformational flexibility suggested by modelling was investigated in DMSO-d_6 through ^{1}H NMR 1D ROESY experiments (Figure 3). When inverting the signal of the amide NH proton (H_c) of macrocycle **1**, a Nuclear Overhauser Effect (NOE) was only observed with phenanthrene proton H_d, consistent with a conformation where all the amide NHs (H_c) are pointing towards the centre of the cavity (Figure 2a). The 1D-ROESY NMR spectrum of macrocycle **2** showed strong NOEs of the NH protons (H_c) with both the azomethine protons H_d and the aromatic protons H_b. A weaker NOE can also be observed with the H_a protons, indicating that the NH can point out of the cavity. The modelling studies showed that macrocycle **2** can adopt conformations with 4, 3, or 2 NH groups pointing into the cavity, conformers which are in fast exchange on the chemical shift time scale, as only a single NH signal is observed in the NMR spectra. Considering that the shortest distances of NH_c to H_a and to H_b are similar in the conformation of lowest energy derived from the modelling studies (Figure 2b), the larger NOE to H_b implies that in solution on average more NH groups point into the cavity than out of it. We noted that upon addition of an excess of $TBAH_2PO_4$ as guest to a solution of macrocycle **2**, the NOE between protons H_c and H_a was no longer observed, while NOEs between H_c and protons H_d and H_b remained visible (Figure S1), suggesting that in the presence of the guest the macrocycle adopts a conformation where all the NH protons are oriented into the binding cavity. With macrocycle **3** the amide protons H_c exhibit strong NOEs with protons H_a and H_b, consistent with the NHs pointing both inside and outside the cavity, as observed in the model (Figure 2c) as well as in the X-ray crystal structure of the macrocycle (Figure S2), which corroborated the H-bond interactions between two of the carbonyls with the two opposite NH groups.

Anion binding

The interaction of macrocycles **1**-**3** with the three anionic guests Cl^-, $H_2PO_4^-$, and $H_2P_2O_7^{2-}$ was studied through ^{1}H-NMR titrations with the corresponding tetrabutylammonium salts in DMSO-d_6 with 0.5% H_2O added. For macrocycles **1** and **2**, the ^{1}H NMR signals of the protons pointing into the cavity showed clear downfield shifts upon addition of TBACl (Figures S3 and S4), while the signals for protons H_c and H_b of macrocycle **3** were shifted less (Figure S5). The displacements of the ^{1}H NMR signals of the protons pointing into the cavity were fitted with a 1:1 binding model[42–44] and $K_{1:1}$ values for Cl^- of $1.2\cdot10^2$ M^{-1} and $2.1\cdot10^3$ M^{-1} were obtained for **1** and **2** respectively (Table 1).

The intramolecular hydrogen bonding observed for macrocycle **3**, both by modelling (Figure 2c) and by X-ray crystallography (Figure S2), probably explains the poor interaction of this macrocycle with Cl^-. The lower affinity of macrocycle **1** for Cl^-, compared to macrocycle **2**, can be explained by the fact that only one of the dipicolinic bisamide motifs is able to interact with Cl^- (Figure 2g). Thus, the affinity of **1** was found to be within the same order of magnitude, albeit slightly higher, as that observed for dipicolinic bisamides with less preorganization (10-47 M^{-1}),[45] but significantly lower than that of more flexible dipicolinic bisamide macrocycles (1930 M^{-1}, in DMSO-d_6).[22] More surprising, however, was the fact that macrocycle **2** exhibits a high affinity for Cl^- compared to, for example, the macrocycles of the same size utilizing four ureas as the binding motifs (up to 500 M^{-1}, in DMSO-d_6),[46] which could have been expected to provide higher affinities than acylhydrazones.[35]

Table 1. Association constants determined for macrocycles **1**, **2**, and **3** in DMSO.

Host	K_a Cl^-		K_a $H_2PO_4^-$	K_a $H_2P_2O_7^{2-}$
	NMR (M^{-1})[a]	UV-Vis (M^{-1})[b]	UV-Vis (M^{-1})[b]	UV-Vis (M^{-1})[b]
1	$K_{1:1}$= (1.2±0.1)·10^2	$K_{1:1}$= 78±4	$K_{1:1}$= (8.9±1.2)·10^2	$K_{1:1}$= (3.9±0.3)·10^3
2	$K_{1:1}$= (2.1±0.3)·10^3	$K_{1:1}$= (1.6±0.1)·10^3	$K_{1:1}$= (1.2±0.8)·10^6 $K_{1:2}$= (5.0±0.5)·10^5	$K_{1:1}$= (6.4±2.6)·10^6
3	$K_{1:1}$= < 10	-[c]	-[c]	-[c]

[a] DMSO-d_6 + 0.5% H_2O, 298 K [b] DMSO, 298 K [c] not determined. The errors are based on the standard deviations of the results from three titrations.

During the ^{1}H-NMR titrations of macrocycle **1** in DMSO (0.5% H_2O) with $H_2PO_4^-$ and $H_2P_2O_7^{2-}$ the signals showed significant broadening after addition of 1-2 equivalents of the salts, preventing a reliable quantification of the binding (Figures S6-7). Additionally, precipitation was observed after addition of 1 equivalent of the salts, further complicating the binding studies. The NH signal of macrocycle **3** also broadened upon addition of $H_2PO_4^-$ and $H_2P_2O_7^{2-}$, while the other signals showed only minimal changes with up to 5 eq. of these salts (Figures S8-9).

In contrast, a set of new signals appeared in the ^{1}H-NMR spectra of macrocycle **2** upon addition of $H_2PO_4^-$ or $H_2P_2O_7^{2-}$, characteristic of slow exchange on the NMR chemical shift timescale, which allowed a more complete analysis of the binding events (Figure 4). The addition of $H_2PO_4^-$ to **2** led to a gradual decrease of the original H_b signal (8.37 ppm), with a new signal appearing at 8.5 ppm ($H_{b'}$) during the first part of the titration (up to 1.3 eq. of $H_2PO_4^-$), which disappeared upon further addition of guest with another signal appearing at 8.9 ppm ($H_{b''}$). This behaviour is indicative of two binding events, the binding of a first guest anion, followed by formation of a 1:2 complex with $H_2PO_4^-$. Such 1:2 complexes have been reported previously and their existence has been attributed to the formation of phosphate dimers involving Anti-Electrostatic Hydrogen Bonds (AEHBs).[47–51]

During the titration, a gradual decrease in the intensity of the H_d azomethine signal at 9.0 ppm was observed concomitant with the appearance of only one new signal $H_{d'}$ at 9.4 ppm. Signal H_c, only showed some broadening when less than 1 eq. of $H_2PO_4^-$ was added and it is only upon further addition of the guest that a new signal appeared at 14.1 ppm ($H_{c'}$), which is clearly visible in the spectrum with 2.1 eq. of $H_2PO_4^-$. The variation of the integration of the H_c and H_d signals upon titration are shown in Figure 4b. The integrations suggest that signal $H_{d'}$ is superposition of this proton's signals in both the 1:1 complex and the 1:2 complex, whereas signal H_c would be the superposition of the signals arising from the 1:1 complex and the free receptor. The first $H_2PO_4^-$ binding event can thus be observed from the azomethine H_d signals and the second event is reflected by the behaviour of the NH_c signals.

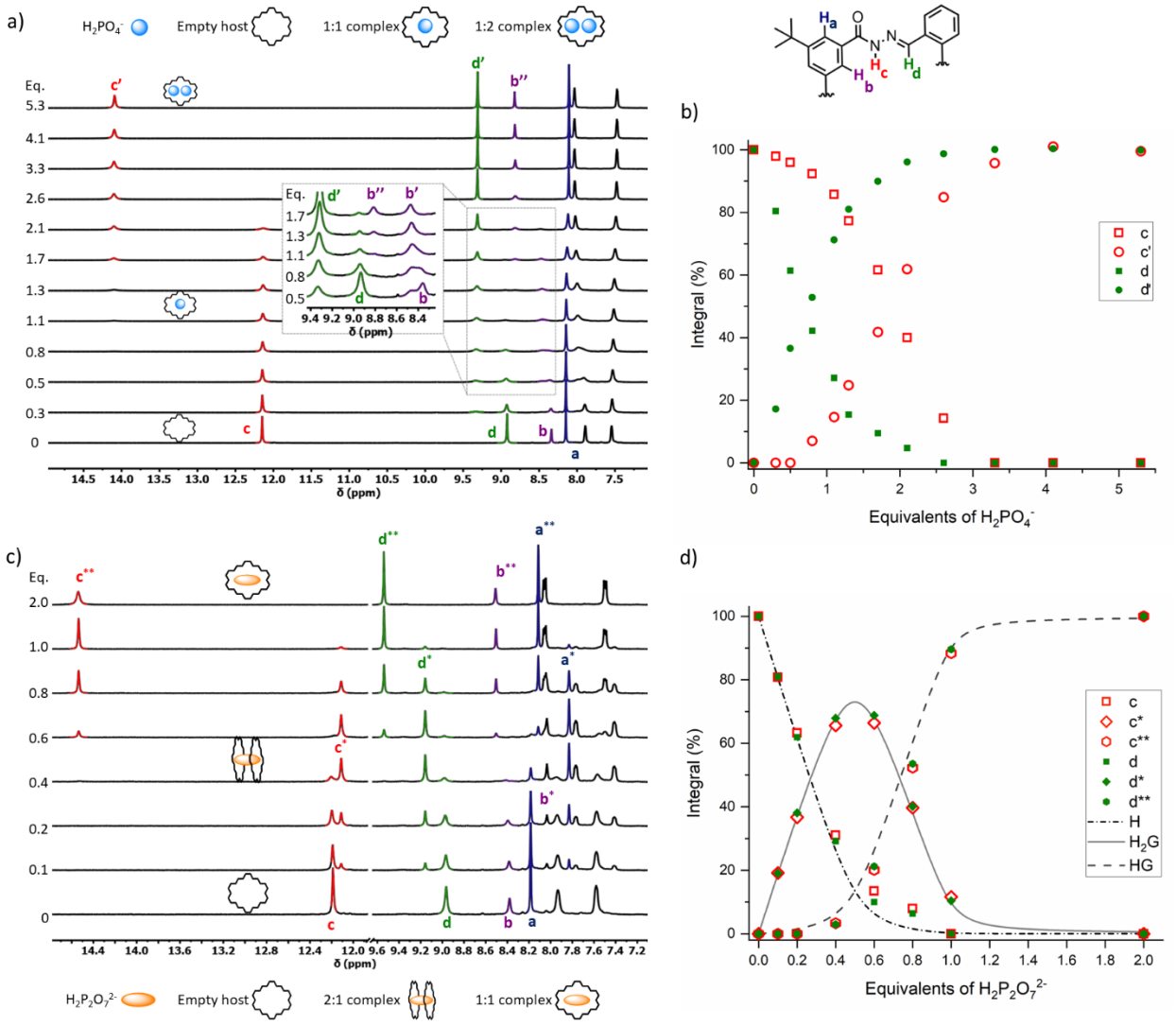

Figure 4. ^{1}H-NMR titrations of macrocycle **2** (1 mM, DMSO-d_6 + 0.5% H_2O) with $TBAH_2PO_4$ (a, 600 MHz), and $TBA_2H_2P_2O_7$ (c, 400 MHz); b) Integrals of signals c, c', d, and d' as % relative to the *tert*-butyl signal over the course of titration with $TBAH_2PO_4$; d) Relative proportions of signals d, d* and d** as well as c, c* and c** throughout the titration with $TBA_2H_2P_2O_7$ as % of the total integrals of d and c with simulated speciation curves of a 2:1 association (1 mM host, $K_{1:1}$= 6.4·10^6 M^{-1}, $K_{2:1}$= 2·10^4 M^{-1}) overlaid to help guide the eye.

Over the course of the titration of macrocycle **2** with $H_2P_2O_7^{2-}$, two distinct complexes were also identified (Figure 4c). Exchange was slow on the NMR chemical shift scale and distinct signals were observed for several protons which could be easily assigned (Figure S12). The ratio between the different complexes could be determined by integration of the signal corresponding to the azomethine H_d or the NH_c (Figure 4d). Crucially, this revealed that, during the first few additions, the amount of new complex formed corresponded to twice the amount of guest added, implying the formation of a 2:1 host-guest complex. Furthermore, the fact that almost complete formation of the second complex takes place once 1 eq. of $H_2P_2O_7^{2-}$ is added implies that the second binding event results in the formation of a strong 1:1 complex.

UV-Vis spectroscopy was used to determine the affinity constants of macrocycles **1** and **2** with $TBAH_2PO_4$ and $TBA_2H_2P_2O_7$ in DMSO. Titrations with TBACl were performed for comparative purposes and fitting with a 1:1 binding model gave affinity constants in agreement with those obtained by the ^{1}H-NMR titrations (see Table 1 and Figures S13-S14). The data from the UV-Vis spectroscopy titrations of **1** with $H_2PO_4^-$ and $H_2P_2O_7^{2-}$ could be fitted with a 1:1 binding model and resulted in affinity constants of 8.9·10^2 and 3.9·10^3 M^{-1} respectively (Figures S15-S16). The UV-Vis spectra from the titration of **2** with $H_2PO_4^-$ show no isosbestic point (Figure 5a and S17) and gave very poor fits when using a 1:1 binding model, while a much better fit was obtained when using a 1:2 binding model (Figure 5a, inset), yielding large K_a values for both the 1:1 and 1:2 association processes (1·10^6

and $5 \cdot 10^5$ M^{-1}). The formation of a 1:2 complex with $H_2PO_4^-$ is in agreement with the findings from the ^1H NMR titration (Figure 4a) as well as the crystal structure (*vide infra*). In the case of the titration of **2** with $H_2P_2O_7^{2-}$, a clear isosbestic point was observed and the data could be fitted to a 1:1 binding model (Figure 5b and S18), giving a $K_{1:1}$ of $6 \cdot 10^6$ M^{-1}. During the ^1H NMR titration, the formation of a 2:1 host-guest complex was observed (at 1 mM), but the 200-fold lower concentration of **2** (5 µM) would decrease the fraction of this complex present in solution.

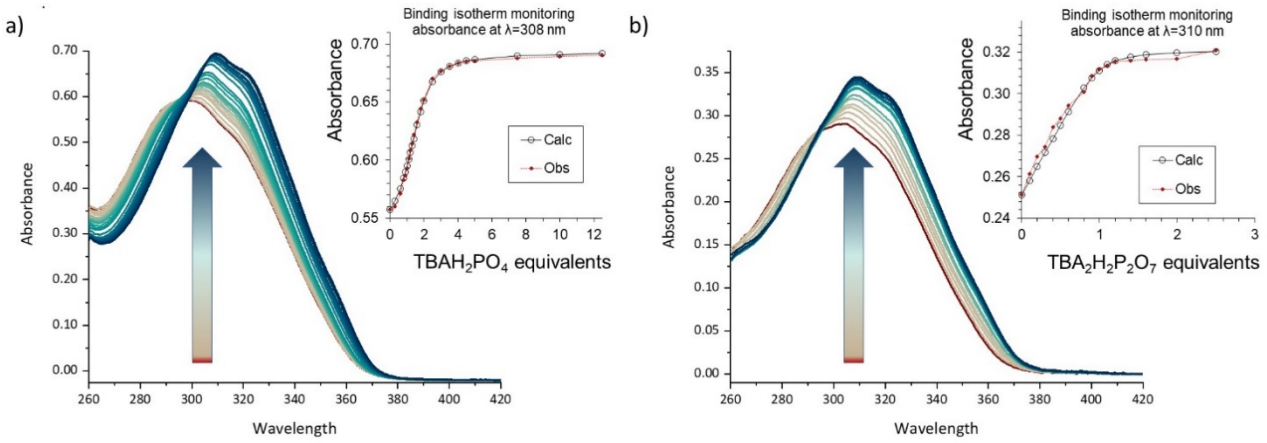

Figure 5. UV-Vis spectroscopy titrations of macrocycle **2** with a) $TBAH_2PO_4$ (10 µM **2** in DMSO) and b) $TBA_2H_2P_2O_7$ (5 µM **2** in DMSO).

As a result, it turns out that macrocycle **2** exhibits the highest affinity of the three macrocycles, regardless of the size of the anion (Table 1). It even outperforms for both Cl^- and $H_2PO_4^-$, the similarly sized tetraurea macrocycles.[46] For macrocycle **3** the lower affinity for the different guests can be explained by the need to outcompete the intramolecular hydrogen bonds that can form in this flexible macrocycle. Flexibility could also explain the difference in affinities between macrocycle **1** and **2** for Cl^- and $H_2PO_4^-$. Both these anions are expected to be too small for macrocycle **1** to optimally exploit all its H-bond donors, whereas macrocycle **2** is most likely able to adapt its conformation so that all H-bond donors can be engaged with each of the anions. More surprising was the fact that macrocycle **2** also outperformed macrocycle **1** in binding $H_2P_2O_7^{2-}$ by three orders of magnitude, since macrocycle **1** was expected to be better preorganized for binding of such larger guests, based on initial computational studies.

X-ray crystallography

To further study the interactions of macrocycle **2** with the different anions, we obtained single crystals of the host-guest systems **2·Cl⁻**, **2·$H_2PO_4^-$**, **2·$H_2P_2O_7^{2-}$**, and **2·malonate** and analysed them by single-crystal X-ray diffraction.

The crystal structure of **2·Cl⁻** showed in the asymmetric unit the presence of two macrocycles adopting a flat conformation (Figure 6a). In each macrocycle, two acylhydrazone groups coordinate to one chloride ion, whereas a water molecule fills the remanent space of the cavity (Figure 6b). In each macrocycle, two N-H···Cl hydrogen bonds are observed between two acylhydrazone groups and the anion with N···Cl distances in the range of 3.325 Å to 3.382 Å. In addition, the water molecule interacts with the remaining acylhydrazone group through the formation of two N-H···O_w hydrogen bonds with N···O_w distances in the range of 3.007 Å to 3.328 Å, supporting the flat conformation of the macrocycle. The presence of both guest molecules in each macrocycle cavity is stabilized by one O_w-H···Cl interaction with O_w···Cl distances of 3.145 Å and 3.191 Å.

In the complex **2·$H_2PO_4^-$**, the macrocycle shows a flat conformation similar to the previous one for **2·Cl⁻**. However, in this case, two molecules of $H_2PO_4^-$ anions are observed in the macrocycle cavity (Figure 6c-d), which corroborates the 1:2 host-guest stoichiometry observed in the binding studies by NMR and UV-Vis titration experiments (Figures 4a and 5a). This association is favored by the formation of two different N-H···O hydrogen bonds with N···O distances of 2.728 Å to 2.785 Å between the anion with the four acylhydrazone groups of the macrocycle. Interestingly, the hydrogen atoms in the $H_2PO_4^-$ anion allow the formation of O-H···O interactions,

with O···O distances of 2.525 Å, between the anions producing a linear polymeric chain running at an angle of 73° to the plane of the macrocycles (Figure 6e).[52,53]

Finally, for the **2·$H_2P_2O_7^{2-}$** complex, a 1:1 ratio between the macrocycle and the anion is observed, favoured by the size of the $H_2P_2O_7^{2-}$ anion, allowing its interaction with all the four acylhydrazone groups. The four different N-H···O hydrogen bonds have a N···O distance in the range of 2.683 Å to 2.825 Å. Once again, the hydrogen atoms in the $H_2P_2O_7^{2-}$ anion allow interactions between anions. Nevertheless, this association was observed for only two anions, forming a dimer rather than a linear network as observed for $H_2PO_4^-$. The crystal lattice of **2·$H_2P_2O_7^{2-}$** can be described as a sandwich-type complex in which two macrocycle molecules surround two anions (Figure 6f-g).[54–56]

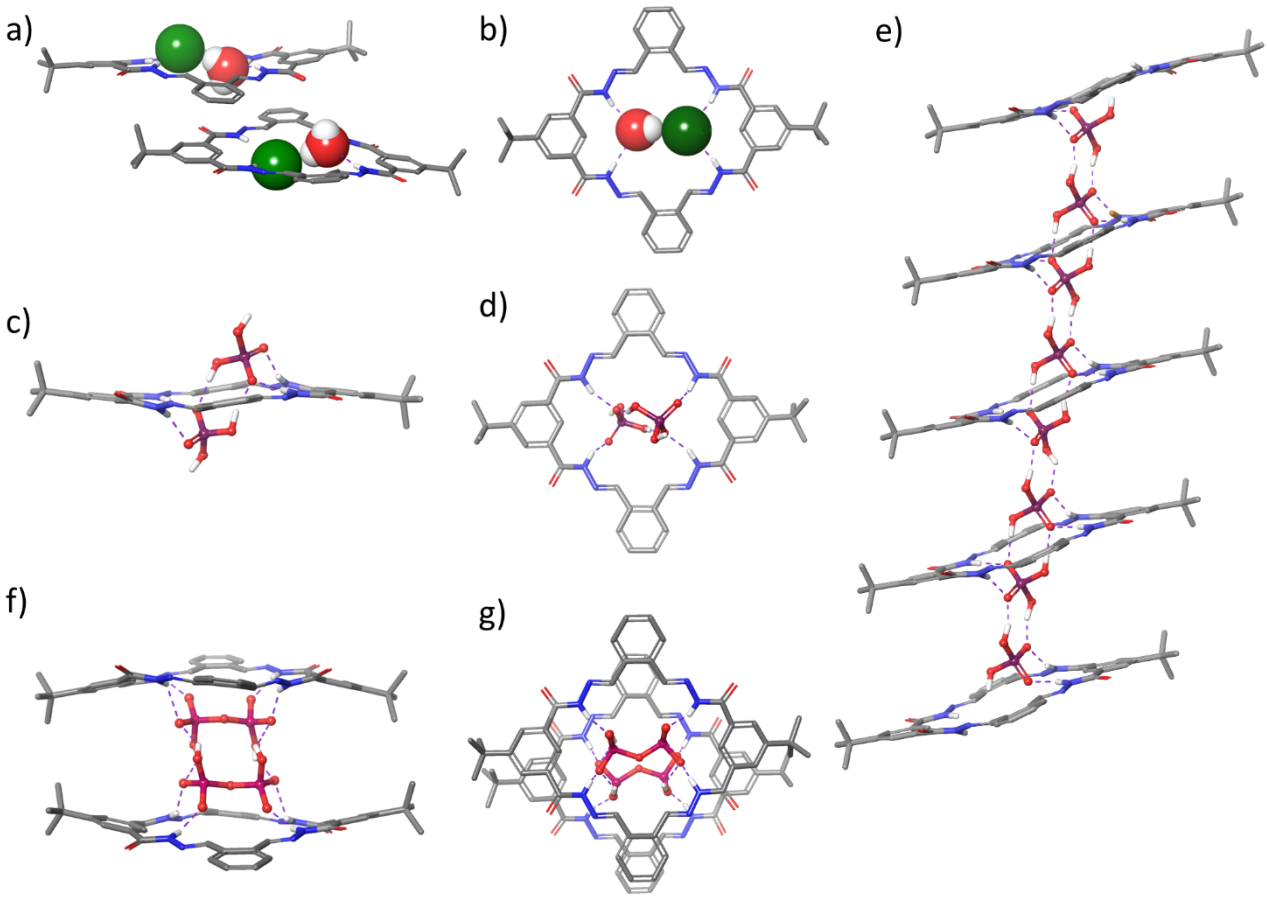

Figure 6. The crystal structures obtained for macrocycle **2** in the presence of Cl^-, $H_2PO_4^-$ and $H_2P_2O_7^{2-}$ in a side on view (a, c, f) and a top down view (b, d, g) as well as a model of the extended structure within the crystal structure of the **2·$H_2PO_4^-$** complex (e). The macrocycle is shown in capped stick representation, $H_2PO_4^-$ and $H_2P_2O_7^{2-}$ are shown in ball and stick representation and H_2O and Cl^- as spacefilled representation. Tetrabutylammonium, solvent molecules not found within the binding cavities, as well as non H-bonding hydrogens are omitted for clarity.

The crystal structure of a complex of **1·Cl^-** was also obtained, showing a chloride and a water molecule bound within the cavity of the macrocycle (Figure 7), similar as for the complex of **2·Cl^-**. In this case however, the macrocycle forms a sandwich complex of two macrocycles, two chloride ions and two water molecules. The macrocycle adopts a saddle conformation to allow it to maintain N···Cl distances between the Cl^- and the amide N-H in the range of 3.22-3.43 Å and N···O_w distances between the water molecule and the amide N-H in the range of 2.93-3.09 Å. The complex is further stabilized by the interaction of the two guest molecules with each other with O_w···Cl distances of 3.19 Å and 3.21 Å as was the case for **2·Cl^-**.

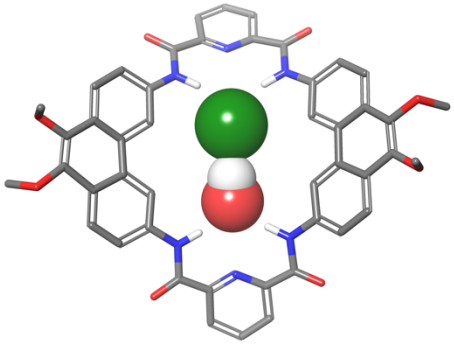

Figure 7. The crystal structure obtained for macrocycle **1** in the presence of Cl^-. The macrocycle is shown in capped stick representation and H_2O and Cl^- as spacefilled representation. Hexyl side chains, Tetrabutylammonium, solvent molecules not found within the binding cavities as well as non H-bonding hydrogens are omitted for clarity.

Conclusion

Three new macrocycles with a 26-membered interior ring size and four NH-based binding moieties have been prepared. The three macrocycles were shown, both by computational modelling as well as 1D-ROESY experiments, to exhibit significantly different degrees of preorganization, originating from different degrees of rigidity within their macrocyclic structures. Through binding studies with anions of varying size (Cl^-, $H_2PO_4^-$, and $H_2P_2O_7^{2-}$) we have shown that the flexibility of a macrocycle can have significant effects on the observed affinities. The flexible macrocycle **3** favours intramolecular hydrogen bonding over interactions with anions. The rigid macrocycle **1** exhibits, not unexpectedly, poor interaction with Cl^- since the cavity was too large, but showed good interactions with $H_2PO_4^-$ and $H_2P_2O_7^{2-}$. Macrocycle **2** exhibits the best anion affinity for all three anions, most likely due to the combination of its preorganization and its ability to adapt its conformation more easily than macrocyclic receptor **1**. X-ray crystallography of complexes of macrocycle **2** with the three anions confirmed its ability to binds these three different anions, of which $H_2PO_4^-$ was bound with a 1:2 host to guest stoichiometry.

These three macrocycles of the same size but varying preorganization and flexibility show that an intermediate flexibility provides the best binding affinity for a range of anions of different size and shape. While several studies reported that more rigidity of preorganized macrocyclic structure provides better affinities, our study illustrates that some flexibility in the macrocycle can be beneficial, in particular for the binding of anions with more complex geometries. This insight will help to guide the design of future generations of macrocyclic receptors for anions or other guests.

Experimental

Synthesis and Characterization. Commercially available solvents and chemical reagents were used as received unless otherwise stated. Purification by Flash Column Chromatography (FCC) was carried out using silica gel with a 60 Å pore size and a particle size of 40-63. Unless otherwise stated, glassware employed for moisture sensitive reactions were flame dried prior to use. NMR spectra were acquired using a Varian VNMRS 400 spectrometer or a JEOL JNM-ECZ400R/S3 operating at 9.4 T (400 MHz for ^1H) equipped with a double resonance OneNMR™ or ROYAL™ probe respectively or a JEOL JNM-ECZ600R/S3 spectrometer operating at 14.1 T (600 MHz for ^1H) equipped with a double resonance ROYAL™ probe. The ^1H spectra were recorded at 298 K unless otherwise stated and, for titration experiments, using a spectral width of 20.0 or 24.0 ppm centred at 5.0 or 6.0 ppm, 3.0 or 4.0 s relaxation delay, 2.43 or 2.6 µs high-power RF pulse width (flip angle of 30°) and 2.2 or 3.0 s acquisition time. Processing was performed using MestReNova 14.3.1-31739. It comprised zero-filling (total of 64k or 256k points), single exponential or cosine square multiplication of the free induction decay, Fourier transform, phase correction, baseline correction, and chemical shift referencing of the spectrum. The ^1H spectra were referenced with respect to the residual signal of the solvent (methanol-d_3: 3.31 ppm; acetone-d_5: 2.05

ppm, DMSO-d_5: 2.50 ppm) and chemical shifts are reported in ppm. Melting points were recorded on a Stuart SMP20 melting points apparatus and are uncorrected. Mass spectrometry was carried out using a QTOF-6520 Agilent instrument.

9,10-bis(hexyloxy)phenanthrene-3,6-diamine dihydrochloride (**7·2(HCl)**). 3,6-dibromo-9,10-dihexoxyphenanthrene **5** (100 mg, 186 µmol), $Pd(dba)_2$ (10.72 mg, 18.65 µmol) and Xphos (35.84 mg, 372 µmol) was mixed in a 5 mL flask and placed under an argon atmosphere. Dry toluene (1 mL) was added and the resulting mixture heated to 80°C followed by addition of benzophenone amine (62.5 µL, 372 µmol). After stirring the solution at 80°C overnight, it was filtered over celite followed by concentration and purification by FCC using 10% EtOAc/Hep as the eluent to yield the crude diimine as a yellow sticky solid. This solid was subsequently dissolved in 1 mL of THF followed by addition of 1 mL of concentrated HCl (37% in H_2O). The resulting precipitate was filtered off on a sintered glass funnel, washed thoroughly with THF (4x 2 mL) and dried in high vacuum to obtain the desired diamine as a white powdery HCl salt (92 mg, 71% over two steps). Decomposition > 210°C. ^{1}H NMR (400 MHz, CD_3OD) δ 8.80 (d, *J* = 2.1 Hz, 2H), 8.44 (d, *J* = 8.8 Hz, 2H), 7.73 (dd, *J* = 8.8, 2.0 Hz, 2H), 4.26 (t, *J* = 6.6 Hz, 4H), 1.99 – 1.87 (m, 4H), 1.67 – 1.54 (m, 4H), 1.46 – 1.35 (m, 8H), 0.99 – 0.89 (m, 6H). ^{13}C{^{1}H} NMR (101 MHz, CD_3OD) δ 144.9, 131.6, 130.3, 129.7, 126.1, 123.6, 118.8, 75.0, 32.8, 31.4, 27.1, 23.7, 14.4. HRMS ($M+H^+$): calc. for $C_{26}H_{37}N_2O_2^+$: 409.2850, found: 409.2858.

Macrocycle 1. To a solution of tetrabutylammonium chloride (2.31 g, 8.31 mmol) in dry DCM (160 mL) under an argon atmosphere was added a solution of pyridine-2,6-dicarbonyl dichloride **8** (41.13 mg, 187 µmol) in dry DCM (20 mL) and a solution containing a mixture of **7·2(HCl)** (90 mg, 187 µmol) and DIPEA (121 mg, 934 µmol) in dry DCM (20 mL) dropwise over the course of 10 hours. After complete addition, the mixture was allowed to stir for an additional 8 hours followed by concentration of the reaction mixture onto celite for purification by FCC, first using 25% acetonitrile/toluene as the eluent to yield the crude macrocycle. A second column using 1% MeOH/DCM as the eluent was employed to obtain the pure macrocycle as an off-white powder (27 mg, 27 %). Mp: > 300°C. ^{1}H NMR (400 MHz, acetone-d_6) δ 10.78 (s, 4H), 8.48 (d, *J* = 7.8 Hz, 4H), 8.45 (d, *J* = 1.9 Hz, 4H), 8.34 (dd, *J* = 8.9, 1.8 Hz, 4H), 8.32 – 8.25 (m, 6H), 4.21 (t, *J* = 6.6 Hz, 8H), 1.97 – 1.88 (m, 8H), 1.65 – 1.55 (m, 8H), 1.46 – 1.37 (m, 16H), 0.97 – 0.91 (m, 12H). ^{13}C{^{1}H} NMR (101 MHz, acetone-d_6) δ 162.2, 149.4, 142.7, 139.5, 135.9, 128.5, 127.1, 125.5, 123.7, 122.7, 115.4, 73.4, 31.7, 30.4, 25.9, 22.5, 13.5. HRMS ($M+K^+$): calc. for $C_{66}H_{74}N_6O_8K^+$: 1117.5200, found: 1117.5164.

Macrocycle 2. Dihydrazide **10** (500 mg, 2 mmol) was suspended in ethanol (100 mL) and heated until a slightly hazy solution was obtained. This solution was then allowed to cool to 35°C and added in one portion to a vigorously stirred mixture of phthalaldehyde (267 mg, 2 mmol) and tetrabutylammonium dihydrogenphosphate (339 mg, 1 mmol) in ethanol (100 mL). After stirring overnight a precipitate had formed which was filtered off on a sintered glass funnel, washed thoroughly with ethanol (8x 15 mL) and dried in high vacuum to yield the desired macrocycle as a white powder (397 mg, 57 %). Mp: Decomposition > 230°C. ^{1}H NMR (400 MHz, DMSO-d_6) δ 12.19 (s, 4H), 8.97 (s, 4H), 8.38 (t, *J* = 1.5 Hz, 2H), 8.19 (d, *J* = 1.5 Hz, 4H), 7.93 (dd, *J* = 5.8, 3.4 Hz, 4H), 7.58 (dd, *J* = 5.9, 3.3 Hz, 4H), 1.41 (s, 18H). ^{13}C{^{1}H} NMR (101 MHz, DMSO-d_6, +3 eq $TBAH_2PO_4$) δ 163.3, 151.1, 144.6, 133.7, 133.7, 129.6, 128.6, 125.7, 123.1, 34.6, 31.0. HRMS ($M+H^+$): calc. for $C_{40}H_{41}N_8O_4^+$: 697.3245, found: 697.3216.

2,2'-(((4,5-diethoxy-1,2-phenylene)bis(methylene))bis(oxy))bis(isoindoline-1,3-dione) (**15**). To a stirred solution of N-hydroxyphthalamide (926 mg, 5.68 mmol) and 1,2-bis(bromomethyl)-4,5-diethoxybenzene **13** (1 g, 2.8 mmol) in dry DMF (15 mL) under argon was added DBU (1 mL, 6.8 mmol) over 5 minutes. Following complete addition, the mixture was left to stir for 25 minutes after which HCl (1N aq. solution, 20 mL) was added and the resulting precipitate filtered on a sintered glass funnel followed by washing with water (3x 10 mL). The wet solid was suspended in toluene for azeotropic removal of water twice over after which the resulting solid was dried in high vacuum to obtain the desired compound as a white solid (1.4 g, 95 %). Mp: Decomposition > 220°C. ^{1}H NMR (400 MHz, DMSO-d_6) δ 7.88 – 7.80 (m, 8H), 7.12 (s, 2H), 5.41 (s, 4H), 4.01 (q, *J* = 7.0 Hz, 4H), 1.27 (t, *J* = 7.0 Hz, 6H). ^{13}C{^{1}H} NMR (101 MHz, DMSO-d_6) δ 163.2, 148.3, 134.8, 128.5, 126.5, 123.2, 116.3, 76.3, 63.8, 14.5. HRMS ($M+H^+$): calc. for $C_{28}H_{25}N_2O_8^+$: 517.1605, found: 517.1591.

O,O'-((4,5-diethoxy-1,2-phenylene)bis(methylene))bis(hydroxylamine) (**16**). To a solution of protected hydroxylamine **15** (400 mg, 774 µmol) in ethanol (5 mL) was added hydrazine hydrate (85 µL, 1.7 mmol) and the resulting mixture stirred overnight at room temperature. The mixture was evaporated onto celite for

purification by FCC using 5% MeOH/DCM as the eluent to yield the desired bis(hydroxylamine) as a white solid (180 mg, 90%) Mp: 104-106°C. ^{1}H NMR (400 MHz, DMSO-d_6) δ 6.89 (s, 2H), 5.97 (s, 2H), 4.55 (s, 4H), 4.01 (q, J = 7.0 Hz, 4H), 1.31 (t, J = 7.0 Hz, 6H). ^{13}C{^{1}H} NMR (101 MHz, DMSO-d_6) δ 147.2, 128.9, 114.6, 74.2, 63.8, 14.8. HRMS (M+H$^+$): calc. for $C_{12}H_{21}N_2O_4^+$: 257.1496, found: 257.1484.

Macrocycle 3. To a stirred solution of tetrabutyl ammonium chloride (108 mg, 390 µmol) and triethylamine (20 µL, 156 µmol) in dry DCM (5 mL) under an argon atmosphere was added solutions of 5-(*tert*-butyl)isophthaloyl dichloride **17** (10.11 mg, 5 mM in dry DCM) and bis(hydroxylamine) **16** (10 mg, 5 mM in dry DCM) dropwise over the course of 30 minutes. The solution was left to stir overnight after which it was evaporated onto celite for purification by FCC using 25 % acetonitrile/toluene to yield the desired macrocycle as a white solid (9.5 mg, 55 %). Mp: Decomposition > 260°C. ^{1}H NMR (400 MHz, DMSO-d_6) δ 12.11 (s, 4H), 8.24 (t, J = 1.6 Hz, 2H), 8.06 (d, J = 1.6 Hz, 4H), 6.97 (s, 4H), 5.07 (s, 8H), 3.92 (q, J = 7.0 Hz, 8H), 1.37 (s, 18H), 1.21 (t, J = 7.0 Hz, 12H). ^{13}C{^{1}H} NMR (101 MHz, DMSO-d_6) δ 163.7, 151.3, 147.7, 132.0, 127.9, 127.3, 123.4, 116.8, 75.1, 63.8, 34.8, 30.9, 14.6. HRMS (M+H$^+$): calc. for $C_{48}H_{61}N_4O_{12}^+$: 885.4280, found: 885.4279.

General procedure for titrations.

^{1}H-NMR. All titrations were carried out at 1 mM macrocycle concentration in DMSO-d_6 with 0.5% H_2O. Stock solutions of guests were prepared using the host solution to ensure that no dilution of the host takes place over the course of the titration. TBA salts were dried under high vacuum prior to the preparation of stock solutions with concentrations in the range of 20-200 mM depending on the titration. Aliquots of guest stock solution were added sequentially to an NMR tube with the free host and a proton spectrum acquired for each addition. The chemical shift of NH protons and other relevant signals were fitted to a 1:1 binding model using Bindfit.[42–44]

UV-Vis. Titrations were carried out at concentration ranges of 5-15 µM in DMSO. Stock solutions of guests were prepared using the host solution to ensure that no dilution of the host takes place over the course of the titration. TBA salts were dried under high vacuum prior to the preparation of stock solutions with concentrations in the range of 0.5-100 mM. Aliquots of guest stock solution were added sequentially to a cuvette with the free host and a UV-Vis absorption spectrum acquired for each addition on a Shimadzu UV-3600 UV-Vis spectrometer at 25°C. The change of absorption at relevant wavelengths were fitted to an appropriate binding model (1:1 or 1:2) using Bindfit.[42–44]

Molecular modelling.

Initial modelling was done by Monte Carlo multiple minimum (MCMM) conformational searches (100 steps per torsion angle, maximum 1000 steps in total), performed in Schrödinger Release 2019-1, using the OPL3e force field without implicit solvation in Maestro MacroModel (version 11.9.011). The structure obtained after this first run of Molecular Mechanics geometry optimization runs were further minimized using the semi-empirical MOPAC2016 package (Version: 22.110W, James J. P. Stewart) using the PM7 Hamiltonian (full coordinates geometry optimization, MM correction to CONH barrier, convergence for gradient norm below 0,10).

X-ray crystallography.

Generally, single crystals were grown from 1-4 ml solutions of macrocycle (1-3 mM). Single crystals of **2·Cl$^-$** were grown by slow evaporation of a dioxane solution of **2** in the presence of excess TBACl. Single crystals of **2·$H_2PO_4^-$** were obtained by slow evaporation of a DMSO/acetone solution of **2** in the presence of excess $TBAH_2PO_4$. Single crystals of **2·$H_2P_2O_7^{2-}$** were obtained by slow evaporation of a chloroform solution of **2** in the presence of excess $TBA_2H_2P_2O_7$. Single crystals of **2** with malonate were obtained by slow evaporation of a dioxane solution of **2** in the presence of excess $TBA_2C_3H_2O_4$. Single crystals of **1·Cl$^-$** were grown by slow evaporation of a chloroform solution of **1** in the presence of excess TBACl. Single crystals of **3** were obtained by slow evaporation of a dioxane solution of **3**.

Diffraction data were collected using the Oxford Diffraction Gemini R Ultra diffractometer (Cu Kα, multilayer mirror, Ruby CCD area detector) at 100(2) K except **2·$H_2PO_4^-$** was collected at 295(2) K. Data collection, unit cells determination and data reduction were carried out using CrysAlis PRO software package[57] using Olex2[58] and shelXle[59], the structure was solved with the SHELXT 2015[60] structure solution program by Intrinsic Phasing

methods and refined by full-matrix least squares on $|F|^2$ using SHELXL-2018/3.[60] Non-hydrogen atoms were refined anisotropically, while C–H hydrogen atoms were placed in geometrically calculated positions using a riding model. Additional details of the refinement are given in the SI. CCDC deposition numbers are 2311610-2311615.

Acknowledgements

The results reported here are part of a project that has received funding from the European Research Council (ERC, Grant agreement No. 802727) and a Marie Skłodowska-Curie fellowship (awarded to Aaron Torres-Huerta, Grant agreement No. 101065037) under the European Union's Horizon 2020 and Horizon Europe research and innovation programmes. Hennie Valkenier is a Research Associate and Karolis Norvaisa is a Postdoctoral Researcher of the Fonds de la Recherche Scientifique – FNRS. We thank the PC2 technological platform at the University of Namur for access to the single-crystal X-ray diffractometer. The authors thank Dr. Koen Robeyns for discussions regarding the refinement of compound **2**·$H_2P_2O_7^{2-}$.

Notes

The authors declare no competing financial interests.

References

(1) Busschaert, N.; Caltagirone, C.; Van Rossom, W.; Gale, P. A. Applications of Supramolecular Anion Recognition. *Chem Rev* **2015**, *115* (15), 8038–8155. https://doi.org/10.1021/acs.chemrev.5b00099.

(2) Jeffery T. Davis; Philip A. Gale; Roberto Quesada. Advances in Anion Transport and Supramolecular Medicinal Chemistry. *Chem Soc Rev* **2020**, *49*, 6056–6086. https://doi.org/10.1039/C9CS00662A.

(3) Assaf, K. I.; Nau, W. M. Large Anion Binding in Water. *Org Biomol Chem* **2023**, *21* (33), 6636–6651. https://doi.org/10.1039/D3OB00975K.

(4) Zhao, J.; Yang, D.; Yang, X.-J.; Wu, B. Anion Coordination Chemistry: From Recognition to Supramolecular Assembly. *Coord Chem Rev* **2019**, *378*, 415–444. https://doi.org/10.1016/j.ccr.2018.01.002.

(5) Takeda, E.; Taketani, Y.; Sawada, N.; Sato, T.; Yamamoto, H. The Regulation and Function of Phosphate in the Human Body. *BioFactors* **2004**, *21* (1–4), 345–355. https://doi.org/10.1002/biof.552210167.

(6) Hruska, K. A.; Mathew, S.; Lund, R.; Qiu, P.; Pratt, R. Hyperphosphatemia of Chronic Kidney Disease. *Kidney Int* **2008**, *74* (2), 148–157. https://doi.org/10.1038/ki.2008.130.

(7) Williams, C. J.; Rosenthal, A. K. Pathogenesis of Calcium Pyrophosphate Deposition Disease. *Best Pract Res Clin Rheumatol* **2021**, *35* (4), 101718. https://doi.org/10.1016/j.berh.2021.101718.

(8) Villa-Bellosta, R. Vascular Calcification: Key Roles of Phosphate and Pyrophosphate. *Int J Mol Sci* **2021**, *22* (24), 13536. https://doi.org/10.3390/ijms222413536.

(9) Orriss, I. R.; Arnett, T. R.; Russell, R. G. G. Pyrophosphate: A Key Inhibitor of Mineralisation. *Curr Opin Pharmacol* **2016**, *28*, 57–68. https://doi.org/10.1016/j.coph.2016.03.003.

(10) Cataldo, A.; Norvaisa, K.; Halgreen, L.; Bodman, S. E.; Bartik, K.; Butler, S. J.; Valkenier, H. Transmembrane Transport of Inorganic Phosphate by a Strapped Calix[4]Pyrrole. *J Am Chem Soc* **2023**, *145* (30), 16310–16314. https://doi.org/10.1021/jacs.3c04631.

(11) Kataev, E. A. Converting PH Probes into "Turn-on" Fluorescent Receptors for Anions. *Chem. Commun.* **2023**, *59* (13), 1717–1727. https://doi.org/10.1039/D2CC06194E.

(12) Pal, S.; Ghosh, T. K.; Ghosh, R.; Mondal, S.; Ghosh, P. Recent Advances in Recognition, Sensing and Extraction of Phosphates: 2015 Onwards. *Coord Chem Rev* **2020**, *405*, 213128. https://doi.org/10.1016/j.ccr.2019.213128.

(13) Anbu, S.; Paul, A.; Stasiuk, G. J.; Pombeiro, A. J. L. Recent Developments in Molecular Sensor Designs for Inorganic Pyrophosphate Detection and Biological Imaging. *Coord Chem Rev* **2021**, *431*, 213744. https://doi.org/10.1016/j.ccr.2020.213744.

(14) Beyeh, N. K.; Díez, I.; Taimoory, S. M.; Meister, D.; Feig, A. I.; Trant, J. F.; Ras, R. H. A.; Rissanen, K. High-Affinity and Selective Detection of Pyrophosphate in Water by a Resorcinarene Salt Receptor. *Chem Sci* **2018**, *9* (5), 1358–1367. https://doi.org/10.1039/C7SC05167K.

(15) Macreadie, L. K.; Gilchrist, A. M.; McNaughton, D. A.; Ryder, W. G.; Fares, M.; Gale, P. A. Progress in Anion Receptor Chemistry. *Chem* **2022**, *8* (1), 46–118. https://doi.org/10.1016/j.chempr.2021.10.029.

(16) Pal, S.; Ghosh, T. K.; Ghosh, R.; Mondal, S.; Ghosh, P. Recent Advances in Recognition, Sensing and Extraction of Phosphates: 2015 Onwards. *Coord Chem Rev* **2020**, *405*, 213128. https://doi.org/10.1016/j.ccr.2019.213128.

(17) Jonathan L Sessler; Philip Gale; Won-Seob Cho. *Anion Receptor Chemistry*; Stoddart, J. F., Ed.; The Royal Society of Chemistry, 2006. https://doi.org/10.1039/9781847552471.

(18) Cram, D. J. The Design of Molecular Hosts, Guests, and Their Complexes (Nobel Lecture). *Angew. Chem., Int. Ed. Engl.* **1988**, *27* (8), 1009–1020. https://doi.org/10.1002/anie.198810093.

(19) Liu, Z.; Nalluri, S. K. M.; Stoddart, J. F. Surveying Macrocyclic Chemistry: From Flexible Crown Ethers to Rigid Cyclophanes. *Chem Soc Rev* **2017**, *46*, 2459–2478. https://doi.org/10.1039/C7CS00185A.

(20) Valkenier, H.; Davis, A. P. Making a Match for Valinomycin: Steroidal Scaffolds in the Design of Electroneutral, Electrogenic Anion Carriers. *Acc Chem Res* **2013**, *46* (12), 2898–2909. https://doi.org/10.1021/ar4000345.

(21) Dietrich, B.; Guilhem, J.; Lehn, J.; Pascard, C.; Sonveaux, E. Molecular Recognition in Anion Coordination Chemistry. Structure, Binding Constants and Receptor-Substrate Complementarity of a

Series of Anion Cryptates of a Macrobicyclic Receptor Molecule. *Helv Chim Acta* **1984**, *67* (1), 91–104. https://doi.org/10.1002/hlca.19840670112.
(22) Chmielewski, M. J.; Jurczak, J. Anion Binding versus Intramolecular Hydrogen Bonding in Neutral Macrocyclic Amides. *Chem - Eur J* **2006**, *12* (29), 7652–7667. https://doi.org/10.1002/chem.200501471.
(23) Chmielewski, M. J.; Jurczak, J. Anion Recognition by Neutral Macrocyclic Amides. *Chem - Eur J* **2005**, *11* (20), 6080–6094. https://doi.org/10.1002/chem.200500232.
(24) Szumna, A.; Jurczak, J. A New Macrocyclic Polylactam-Type Neutral Receptor for Anions - Structural Aspects of Anion Recognition. *European J Org Chem* **2001**, No. 21, 4031–4039. https://doi.org/10.1002/1099-0690(200111)2001:21<4031::AID-EJOC4031>3.0.CO;2-9.
(25) Liu, W.; Oliver, A. G.; Smith, B. D. Stabilization and Extraction of Fluoride Anion Using a Tetralactam Receptor. *J. Org. Chem.* **2019**, *84* (7), 4050–4057. https://doi.org/10.1021/acs.joc.9b00042.
(26) Hua, Y.; Ramabhadran, R. O.; Karty, J. A.; Raghavachari, K.; Flood, A. H. Two Levels of Conformational Pre-Organization Consolidate Strong CH Hydrogen Bonds in Chloride–Triazolophane Complexes. *Chem. Commun.* **2011**, *47* (21), 5979–5981. https://doi.org/10.1039/c1cc10428d.
(27) Glas, A.; Wamhoff, E.; Krüger, D. M.; Rademacher, C.; Grossmann, T. N. Increased Conformational Flexibility of a Macrocycle – Receptor Complex Contributes to Reduced Dissociation Rates. *Chem. Eur. J.* **2017**, *23*, 16157–16161. https://doi.org/10.1002/chem.201702776.
(28) Yi, R.; Liu, X. L.; Tang, Z. H.; Huang, C.; Zhu, B. X.; Zhu, C. Anion Binding Properties for Pyrophosphate Derived from a 2,6-Diamidopyridinedipyrromethane Macrocycle. *Chem. Pap.* **2021**, *75* (8), 4405–4411. https://doi.org/10.1007/s11696-021-01554-6.
(29) Sessler, J. L.; Cai, J.; Gong, H. Y.; Yang, X.; Arambula, J. F.; Hay, B. P. A Pyrrolyl-Based Triazolophane: A Macrocyclic Receptor with CH and NH Donor Groups That Exhibits a Preference for Pyrophosphate Anions. *J Am Chem Soc* **2010**, *132* (40), 14058–14060. https://doi.org/10.1021/ja107098r.
(30) Hunter, C. A.; Purvis, D. H. A Binary Quinone Receptor. *Angew Chem, Int Ed Engl* **1992**, *31* (6), 792–795. https://doi.org/10.1002/anie.199207921.
(31) Malone, J. F.; Murray, C. M.; Dolan, G. M.; Docherty, R.; Lavery, A. J. Intermolecular Interactions in the Crystal Chemistry of N,N′-Diphenylisophthalamide, Pyridine-2,6-Dicarboxylic Acid Bisphenylamide, and Related Compounds. *Chem. Mater.* **1997**, *9* (12), 2983–2989. https://doi.org/10.1021/cm970350t.
(32) Bryantsev, V. S.; Hay, B. P. Are C-H Groups Significant Hydrogen Bonding Sites in Anion Receptors? Benzene Complexes with Cl-, NO3-, and ClO 4-. *J Am Chem Soc* **2005**, *127* (23), 8282–8283. https://doi.org/10.1021/ja0518272.
(33) Kavallieratos, K.; Bertao, C. M.; Crabtree, R. H. Hydrogen Bonding in Anion Recognition: A Family of Versatile, Nonpreorganized Neutral and Acyclic Receptors. *J Org Chem* **1999**, *64* (5), 1675–1683. https://doi.org/10.1021/jo982382l.
(34) Yamnitz, C. R.; Negin, S.; Carasel, I. A.; Winter, R. K.; Gokel, G. W. Dianilides of Dipicolinic Acid Function as Synthetic Chloride Channels. *Chem. Commun.* **2010**, *46* (16), 2838–2840. https://doi.org/10.1039/b924812a.
(35) Martínez-Crespo, L.; Halgreen, L.; Soares, M.; Marques, I.; Félix, V.; Valkenier, H. Hydrazones in Anion Transporters: The Detrimental Effect of a Second Binding Site. *Org Biomol Chem* **2021**, *19* (38), 8324–8337. https://doi.org/10.1039/D1OB01279G.
(36) Mansoori, Y.; Koohi-Zargar, B.; Shekaari, H.; Zamanloo, M. R.; Imanzadeh, G. H. Polyamides with Pendant 1,3,4-Oxadiazole and Pyridine Moieties. *Chin. J. Polym. Sci.* **2012**, *30* (1), 112–121. https://doi.org/10.1007/s10118-012-1092-8.
(37) Maran, U.; Conley, H.; Frank, M.; Arif, A. M.; Orendt, A. M.; Britt, D.; Hlady, V.; Davis, R.; Stang, P. J. Giant Micelles of Organoplatinum(II) Gemini Amphiphiles. *Langmuir* **2008**, *24* (10), 5400–5410. https://doi.org/10.1021/la800136p.
(38) Sakurai, M.; Kihara, N. Thermally Stable Diels–Alder Polymer Using an Azodicarbonyl Compound as the Dienophile. *Polymer* **2019**, *167*, 60–66. https://doi.org/10.1016/j.polymer.2019.01.071.
(39) Heim, C.; Affeld, A.; Nieger, M.; Vögtle, F. Size Complementarity of Macrocyclic Cavities and Stoppers in Amide- Rotaxanes. *Helv Chim Acta* **1999**, *82* (5), 746–759. https://doi.org/10.1002/(SICI)1522-2675(19990505)82:5<746::AID-HLCA746>3.0.CO;2-C.

(40) Suzuki, R.; Konno, H. Stain Protocol for the Detection of N-Terminal Amino Groups during Solid-Phase Peptide Synthesis. *Org. Lett.* **2020**, *22* (9), 3309–3312. https://doi.org/10.1021/acs.orglett.0c00445.
(41) Meng, X.; Xu, Q.; Zhang, W.; Tan, Z.; Li, Y.; Zhang, Z.; Jiang, L.; Shu, C.; Wang, C. Effects of Alkoxy Chain Length in Alkoxy-Substituted Dihydronaphthyl-Based [60]Fullerene Bisadduct Acceptors on Their Photovoltaic Properties. *ACS Appl Mater Interfaces* **2012**, *4* (11), 5966–5973. https://doi.org/10.1021/am301629d.
(42) *supramolecular.org*. http://supramolecular.org (accessed 2023-01-20).
(43) Brynn Hibbert, D.; Thordarson, P. The Death of the Job Plot, Transparency, Open Science and Online Tools, Uncertainty Estimation Methods and Other Developments in Supramolecular Chemistry Data Analysis. *Chem. Commun.* **2016**, *52* (87), 12792–12805. https://doi.org/10.1039/c6cc03888c.
(44) Thordarson, P. Determining Association Constants from Titration Experiments in Supramolecular Chemistry. *Chem Soc Rev* **2011**, *40* (3), 1305–1323. https://doi.org/10.1039/c0cs00062k.
(45) Picci, G.; Carreira-barral, I.; Alonso-carrillo, D.; Sanz-González, D.; Fernández-López, P.; García-Valverde, M.; Caltagirone, C.; Quesada, R. Simple Isophthalamides / Dipicolineamides as Active Transmembrane Anion Transporters. *Supramol Chem* **2019**, *32* (2), 112–118. https://doi.org/https://doi.org/10.1080/10610278.2019.1702194.
(46) Snellink-Ruël, B. H. M.; Antonisse, M. M. G.; Engbersen, J. F. J.; Timmerman, P.; Reinhoudt, D. N. Neutral Anion Receptors with Multiple Urea-Binding Sites. *European J Org Chem* **2000**, No. 1, 165–170. https://doi.org/10.1002/(sici)1099-0690(200001)2000:1<165::aid-ejoc165>3.0.co;2-#.
(47) Zhao, W.; Flood, A. H.; White, N. G. Recognition and Applications of Anion–Anion Dimers Based on Anti-Electrostatic Hydrogen Bonds (AEHBs). *Chem Soc Rev* **2020**, *49* (22), 7893–7906. https://doi.org/10.1039/D0CS00486C.
(48) He, Q.; Tu, P.; Sessler, J. L. Supramolecular Chemistry of Anionic Dimers, Trimers, Tetramers, and Clusters. *Chem* **2018**, *4* (1), 46–93. https://doi.org/10.1016/j.chempr.2017.10.015.
(49) Valiyaveettil, S.; Engbersen, J. F. J.; Verboom, W.; Reinhoudt, D. N. Synthesis and Complexation Studies of Neutral Anion Receptors. *Angew Chem, Int Ed Engl* **1993**, *32* (6), 900–901. https://doi.org/10.1002/anie.199309001.
(50) Mungalpara, D.; Kelm, H.; Valkonen, A.; Rissanen, K.; Keller, S.; Kubik, S. Oxoanion Binding to a Cyclic Pseudopeptide Containing 1,4-Disubstituted 1,2,3-Triazole Moieties. *Org Biomol Chem* **2017**, *15* (1), 102–113. https://doi.org/10.1039/C6OB02172G.
(51) Pramanik, S.; Thordarson, P.; Day, V. W.; Bowman-James, K. Oligomeric Phosphate Clusters in Macrocyclic Channels. *CrystEngComm* **2022**, *24* (46), 8047–8051. https://doi.org/10.1039/D2CE00756H.
(52) Fatila, E. M.; Pink, M.; Twum, E. B.; Karty, J. A.; Flood, A. H. Phosphate-Phosphate Oligomerization Drives Higher Order Co-Assemblies with Stacks of Cyanostar Macrocycles. *Chem Sci* **2018**, *9* (11), 2863–2872. https://doi.org/10.1039/c7sc05290a.
(53) Rajbanshi, A.; Wan, S.; Custelcean, R. Dihydrogen Phosphate Clusters: Trapping H2PO4– Tetramers and Hexamers in Urea-Functionalized Molecular Crystals. *Cryst Growth Des* **2013**, *13* (5), 2233–2237. https://doi.org/10.1021/cg400336q.
(54) Deliomeroglu, M. K.; Lynch, V. M.; Sessler, J. L. Non-Cyclic Formylated Dipyrromethanes as Phosphate Anion Receptors. *Chem Sci* **2016**, *7* (6), 3843–3850. https://doi.org/10.1039/C6SC00015K.
(55) Mungalpara, D.; Valkonen, A.; Rissanen, K.; Kubik, S. Efficient Stabilisation of a Dihydrogenphosphate Tetramer and a Dihydrogenpyrophosphate Dimer by a Cyclic Pseudopeptide Containing 1,4-Disubstituted 1,2,3-Triazole Moieties. *Chem Sci* **2017**, *8* (9), 6005–6013. https://doi.org/10.1039/C7SC02700A.
(56) He, Q.; Kelliher, M.; Bähring, S.; Lynch, V. M.; Sessler, J. L. A Bis-Calix[4]Pyrrole Enzyme Mimic That Constrains Two Oxoanions in Close Proximity. *J Am Chem Soc* **2017**, *139* (21), 7140–7143. https://doi.org/10.1021/jacs.7b02329.
(57) CrysAlisPro Software System. Rigaku Oxford Diffraction 2020.
(58) Dolomanov, O. V.; Bourhis, L. J.; Gildea, R. J.; Howard, J. A. K.; Puschmann, H. *OLEX2* : A Complete Structure Solution, Refinement and Analysis Program. *J. Appl. Cryst.* **2009**, *42* (2), 339–341. https://doi.org/10.1107/S0021889808042726.

(59) Hübschle, C. B.; Sheldrick, G. M.; Dittrich, B. *ShelXle* : A Qt Graphical User Interface for *SHELXL*. *J. Appl. Cryst.* **2011**, *44* (6), 1281–1284. https://doi.org/10.1107/S0021889811043202.
(60) Sheldrick, G. M. *SHELXT* – Integrated Space-Group and Crystal-Structure Determination. *Acta Cryst.* **2015**, *71* (1), 3–8. https://doi.org/10.1107/S2053273314026370.